

A double double-porosity model for wave propagation in patchy-saturated tight sandstone with fabric heterogeneity

Jing Ba^{1,2*}, Mengqiu Guo¹, Wenhao Xu², Fengyuan Sun², Lin Zhang¹, and Wei Cheng¹
Hohai University, jba@hhu.edu.cn¹, Xi'an Jiaotong University²

SUMMARY

In natural reservoir rocks, fabric heterogeneity can further induce heterogeneous geometrical distribution of immiscible multi-phase fluid mixture, since fluid migration may be affected by lithological variation (mainly permeability) in geological time scales, causing patchy saturation of fluids. Both structure heterogeneity and patchy-saturation can lead to strong seismic wave dispersion and attenuation. In this work, a double double-porosity model is presented to describe the overlapping effect of the two heterogeneities on wave dispersion and attenuation. The wave propagation equations are derived from the Hamilton's principle, and the numerical results for a tight sandstone are compared with corresponding low-frequency experimental data, which shows good agreements. This new model allows for a comprehensive description of wave propagation process in highly complex reservoirs.

Key words: fabric heterogeneity, seismic wave dispersion and attenuation, a double double-porosity model, tight sandstone

INTRODUCTION

It has been widely accepted that the wave-induced local fluid flow (WILFF) could cause significant dispersion and attenuation of compressional waves in sedimentary rocks (Ba et al., 2016; Spencer and Shine, 2016). The two basic aspects for WILFF have been widely studied in the literature. The first aspect is fabric heterogeneity. When seismic wave propagates through rock skeleton, pore fluid will flow from softer pores to stiffer pores since the wave squeezes rock skeleton, resulting in wave relaxation and accompanied attenuation (type I is used here to denote the WILFF related to fabric heterogeneity). The second is patchy-saturation of immiscible fluids. In the rocks with the same compressibility but containing different fluids, pressure gradient will be induced under wave excitations (type II is used for patchy-saturation). Most previous literatures only consider one single aspect of the two heterogeneities.

Marko and Nur (1975) first discussed the type I anelasticity by proposing a model with a liquid-filled flat crack. Pride et al. (2004) presented a double-porosity theory to model the WILFF with mesoscopic heterogeneity, which assumes that the sand aggregates with a size larger than grain but much smaller than the seismic wavelength are embedded into the host sandstone. Ba et al. (2011, 2014) derived a series of exact wave propagation equations for double-porosity rocks with mesoscopic heterogeneity, which are referred to as Biot-Rayleigh (BR) theory.

White (1975) first studied the type II anelasticity by introducing a patchy-saturation model in which a spherical gas pocket is embedded in a concentric sphere shell. Dutta and Odé (1979) reformulated White's model and thus gave a set of more mathematically rigorous wave dynamic equations. Ba et al. (2015) generalized the BR theory from the situation of two porous components saturated with one single fluid to the situation of one single porous component saturated with two immiscible fluids.

The heterogeneities of fabric structure and patchy-saturation commonly coexist in natural reservoir rocks (type III is used here for this overlapping heterogeneity). Therefore, it is essential to further study the overlapping effect of the two heterogeneities. In this work, a double double-porosity (DDP) model is presented to analyze the type III anelasticity. In the case study of tight sandstone, the compressional wave velocity and attenuation at different frequencies and different saturations are predicted accordingly, in comparison with the experimental data.

Double double-porosity theory for wave propagation

The governing equations of wave motion are derived based on the Hamilton's principle. By introducing the fluid variations in WILFF, the local fluid flow interaction is incorporated in the strain energy, kinetic energy and dissipation functions. According to the BR theory, the corresponding local fluid flow governing equation is derived. The equations of wave propagation are

$$\begin{aligned}
& N\nabla^2\mathbf{u} + (A+N)\nabla e + Q_1\nabla\left(\xi^{(1)} + \phi_2\zeta_{12} + \phi_3\zeta_{13}\right) \\
& + Q_2\nabla\left(\xi^{(2)} - \phi_1\zeta_{12} + \phi_4\zeta_{24}\right) \\
& + Q_3\nabla\left(\xi^{(3)} - \phi_1\zeta_{13}\right) + Q_4\nabla\left(\xi^{(4)} - \phi_2\zeta_{24}\right) \\
& = \rho_{00}\ddot{\mathbf{u}} + \rho_{01}\ddot{\mathbf{U}}^{(1)} + \rho_{02}\ddot{\mathbf{U}}^{(2)} + \rho_{03}\ddot{\mathbf{U}}^{(3)} \\
& + \rho_{04}\ddot{\mathbf{U}}^{(4)} + b_1(\dot{\mathbf{u}} - \dot{\mathbf{U}}^{(1)}) + b_2(\dot{\mathbf{u}} - \dot{\mathbf{U}}^{(2)}) \\
& + b_3(\dot{\mathbf{u}} - \dot{\mathbf{U}}^{(3)}) + b_4(\dot{\mathbf{u}} - \dot{\mathbf{U}}^{(4)})
\end{aligned} \tag{1a}$$

$$Q_1\nabla e + R_1\nabla\left(\xi^{(1)} + \phi_2\zeta_{12} + \phi_3\zeta_{13}\right) = \rho_{01}\ddot{\mathbf{u}} + \rho_{11}\ddot{\mathbf{U}}^{(1)} - b_1(\dot{\mathbf{u}} - \dot{\mathbf{U}}^{(1)}), \tag{1b}$$

$$Q_2\nabla e + R_2\nabla\left(\xi^{(2)} - \phi_1\zeta_{12} + \phi_4\zeta_{24}\right) = \rho_{02}\ddot{\mathbf{u}} + \rho_{22}\ddot{\mathbf{U}}^{(2)} - b_2(\dot{\mathbf{u}} - \dot{\mathbf{U}}^{(2)}), \tag{1c}$$

$$Q_3\nabla e + R_3\nabla\left(\xi^{(3)} - \phi_1\zeta_{13}\right) = \rho_{03}\ddot{\mathbf{u}} + \rho_{33}\ddot{\mathbf{U}}^{(3)} - b_3(\dot{\mathbf{u}} - \dot{\mathbf{U}}^{(3)}), \tag{1d}$$

$$Q_4\nabla e + R_4\nabla\left(\xi^{(4)} - \phi_2\zeta_{24}\right) = \rho_{04}\ddot{\mathbf{u}} + \rho_{44}\ddot{\mathbf{U}}^{(4)} - b_4(\dot{\mathbf{u}} - \dot{\mathbf{U}}^{(4)}), \tag{1e}$$

$$\begin{aligned}
& \phi_2\left(Q_1e + R_1\left(\xi^{(1)} + \phi_2\zeta_{12} + \phi_3\zeta_{13}\right)\right) \\
& - \phi_1\left(Q_2e + R_2\left(\xi^{(2)} - \phi_1\zeta_{12} + \phi_4\zeta_{24}\right)\right) \\
& = \frac{1}{3}\rho_f^{(1)}\zeta_{12}R_{12}^2\frac{\phi_1^2\phi_2^2\phi_{20}}{\phi_{10}(\phi_2 + \phi_4)} + \frac{1}{3}\zeta_{12}R_{12}^2\frac{\eta_f^{(1)}\phi_1^2\phi_2^2\phi_{20}}{\kappa_1(\phi_2 + \phi_4)}
\end{aligned} \tag{1f}$$

$$\begin{aligned}
& \phi_3\left(Q_1e + R_1\left(\xi^{(1)} + \phi_2\zeta_{12} + \phi_3\zeta_{13}\right)\right) - \phi_1\left(Q_3e + R_3\left(\xi^{(2)} - \phi_1\zeta_{13}\right)\right) \\
& = \frac{1}{3}\rho_f^{(1)}\zeta_{13}R_{13}^2\phi_1^2\phi_3 + \frac{1}{3}\zeta_{13}R_{13}^2\frac{\eta_f^{(1)}\phi_1^2\phi_3\phi_{10}}{\kappa_1}
\end{aligned} \tag{1g}$$

$$\begin{aligned}
& \phi_4\left(Q_2e + R_2\left(\xi^{(2)} - \phi_1\zeta_{12} + \phi_4\zeta_{24}\right)\right) - \phi_2\left(Q_4e + R_4\left(\xi^{(4)} - \phi_2\zeta_{24}\right)\right) \\
& = \frac{1}{3}\rho_f^{(1)}\zeta_{24}R_{24}^2\phi_2^2\phi_4 + \frac{1}{3}\zeta_{24}R_{24}^2\frac{\eta_f^{(1)}\phi_2^2\phi_4\phi_{20}}{\kappa_2}
\end{aligned} \tag{1h}$$

Where \mathbf{u} , $\mathbf{U}^{(1)}$, $\mathbf{U}^{(2)}$, $\mathbf{U}^{(3)}$ and $\mathbf{U}^{(4)}$ denote the average particle displacements of solid frame, fluid phase 1 (host fluid in host skeleton), fluid phase 2 (host fluid in inclusions), fluid phase 3 (patchy fluid in host skeleton) and fluid phase 4 (patchy fluid in inclusions), respectively. R_{12} , R_{13} and R_{24} refer to the radii of inclusions, pockets in host skeleton and pockets in inclusions. ζ_{12} , ζ_{13} and ζ_{24} are fluid variations in the local fluid flow. ϕ_{10} and ϕ_{20} are the absolute porosities of the host skeleton and inclusions. ϕ_1 , ϕ_2 , ϕ_3 and ϕ_4 are the relative porosities for the four fluid phases. κ_1 and κ_2 are the permeabilities of the host skeleton and inclusions, respectively.

In equation (1), there are nine density coefficients and ten stiffness coefficients that need to be determined. The calculation of density coefficients is based on Ba et al. (2011) (for a double-porosity medium), and

$$\rho_{11} = \alpha_{10}\phi_1\rho_f^{(1)}, \tag{2a}$$

$$\rho_{22} = \alpha_{20}\phi_2\rho_f^{(1)}, \tag{2b}$$

$$\rho_{33} = \alpha_{10}\phi_3\rho_f^{(2)}, \tag{2c}$$

$$\rho_{44} = \alpha_{20}\phi_4\rho_f^{(2)}, \tag{2d}$$

$$\rho_{01} = \phi_1\rho_f^{(1)} - \rho_{11}, \tag{2e}$$

$$\rho_{02} = \phi_2\rho_f^{(1)} - \rho_{22}, \tag{2f}$$

$$\rho_{03} = \phi_3\rho_f^{(2)} - \rho_{33}, \tag{2g}$$

$$\rho_{04} = \phi_4\rho_f^{(2)} - \rho_{44}, \tag{2h}$$

$$\rho_{00} = (1-\phi)\rho_S - \rho_{01} - \rho_{02} - \rho_{03} - \rho_{04}, \tag{2i}$$

Where ϕ is the total porosity of rock skeleton, ρ_s is the density of grain mass, α_{10} and α_{20} refer to the tortuosities of pores in the host skeleton and inclusions, respectively.

The stiffness coefficients are derived by use of the gedanken experiments (Ba et al., 2011) as

$$N = \mu_b, \quad (3a)$$

$$A = (1-\phi)K_s - \frac{2}{3}N - \frac{\beta\phi_1(1-\phi-K_b/K_s)K_s^2/K_f^{(1)}}{\beta(1-\phi-K_b/K_s)+K_s/K_f^{(1)}[\beta(\phi_1+\phi_3)+\phi_2+\phi_4]} - \frac{\phi_2(1-\phi-K_b/K_s)K_s^2/K_f^{(1)}}{(1-\phi-K_b/K_s)+K_s/K_f^{(1)}[\beta(\phi_1+\phi_3)+\phi_2+\phi_4]} - \frac{\beta\phi_3(1-\phi-K_b/K_s)K_s^2/K_f^{(2)}}{\beta(1-\phi-K_b/K_s)+K_s/K_f^{(2)}[\beta(\phi_1+\phi_3)+\phi_2+\phi_4]} - \frac{\phi_4(1-\phi-K_b/K_s)K_s^2/K_f^{(2)}}{(1-\phi-K_b/K_s)+K_s/K_f^{(2)}[\beta(\phi_1+\phi_3)+\phi_2+\phi_4]}, \quad (3b)$$

$$Q_1 = \frac{\beta(1-\phi-K_b/K_s)\phi_1K_s}{\beta(1-\phi-K_b/K_s)+K_s/K_f^{(1)}[\beta(\phi_1+\phi_3)+\phi_2+\phi_4]}, \quad (3c)$$

$$Q_2 = \frac{(1-\phi-K_b/K_s)\phi_2K_s}{(1-\phi-K_b/K_s)+K_s/K_f^{(1)}[\beta(\phi_1+\phi_3)+\phi_2+\phi_4]}, \quad (3d)$$

$$Q_3 = \frac{\beta(1-\phi-K_b/K_s)\phi_3K_s}{\beta(1-\phi-K_b/K_s)+K_s/K_f^{(2)}[\beta(\phi_1+\phi_3)+\phi_2+\phi_4]}, \quad (3e)$$

$$Q_4 = \frac{(1-\phi-K_b/K_s)\phi_4K_s}{(1-\phi-K_b/K_s)+K_s/K_f^{(2)}[\beta(\phi_1+\phi_3)+\phi_2+\phi_4]}, \quad (3f)$$

$$R_1 = \frac{[\beta(\phi_1+\phi_3)+\phi_2+\phi_4]\phi_1K_s}{\beta(1-\phi-K_b/K_s)+K_s/K_f^{(1)}[\beta(\phi_1+\phi_3)+\phi_2+\phi_4]}, \quad (3g)$$

$$R_2 = \frac{[\beta(\phi_1+\phi_3)+\phi_2+\phi_4]\phi_2K_s}{(1-\phi-K_b/K_s)+K_s/K_f^{(1)}[\beta(\phi_1+\phi_3)+\phi_2+\phi_4]}, \quad (3h)$$

$$R_3 = \frac{[\beta(\phi_1+\phi_3)+\phi_2+\phi_4]\phi_3K_s}{\beta(1-\phi-K_b/K_s)+K_s/K_f^{(2)}[\beta(\phi_1+\phi_3)+\phi_2+\phi_4]}, \quad (3i)$$

$$R_4 = \frac{[\beta(\phi_1+\phi_3)+\phi_2+\phi_4]\phi_4K_s}{(1-\phi-K_b/K_s)+K_s/K_f^{(2)}[\beta(\phi_1+\phi_3)+\phi_2+\phi_4]}, \quad (3j)$$

Where μ_b is the shear modulus of dry-rock, K_s is the modulus of grain, K_b is the bulk modulus of rock matrix, $K_f^{(1)}$ and $K_f^{(2)}$ refer to the bulk moduli of the host fluid and patchy fluid, respectively.

Case study of tight gas sandstone

Double double-porosity model is used to analyze the partial-saturation experimental data of a tight sandstone sample (sample TS), and the rock porosity/dry density/permeability are 15%/2.25g·cm⁻³/1mD. The sample is moderately sorted and the minerals are mainly quartz and debris (including siltstones, clay, phyllite, feldspar and mica fragments). Generally, it has low porosity and low permeability, but there still are some less-consolidated sands with higher porosity and permeability in the main rock skeleton.

The wave velocities of the sample are measured with low-frequency measurement techniques (Batzle et al., 2006) at seismic frequencies (10¹-10³Hz), temperature of 20°C, confining pressure of 14MPa and pore pressure of 3.5MPa. In particular, the stress-strain approach is utilized, where the strain due to a low-frequency sinusoidal stress is measured and the rock bulk and shear moduli are thereby estimated. Measurements of full air, butane and water saturation are performed. And two sets of measurement data are obtained as a result of two different sets of gauges.

The bulk and shear moduli of the dry rock are taken as 8.37GPa and 8.22GPa, respectively. The bulk modulus of the less-consolidated sand is determined as 0.13GPa, based on the properties of loose-contact granular material, which leads to the observed strongest dispersion. The density ρ_s and grain modulus K_s of the mineral mixture are 2.65g/cm³ and 22GPa, respectively. Based on the mineral content of the rock samples from the target formation, it is assumed that the sandstone contains $V_2 = 7.5\%$ of less-consolidated components and the inclusion frame has a porosity $\phi_{20} = 0.25$. The radius of the inclusion is set as $R_{12} = 4\text{mm}$ that is larger than the grain size and enables an explanation of the low-frequency dispersion. The porosity of host frame is determined as $\phi_{10} = 0.142$. For the gas pocket in the host frame, the radius is taken as $R_{13} = 200\mu\text{m}$ and the corresponding saturation of host fluid is taken as $S_1 = 0.95$. For the gas pocket in the less-consolidated sand, the radius is taken as $R_{24} = 1\text{mm}$ and the corresponding saturation of host fluid is taken as $S_2 = 0.7$. The four relative porosities are calculated as $\phi_1 = v_1 S_1 \phi_{10}$, $\phi_2 = v_2 S_2 \phi_{20}$, $\phi_3 = v_1 (1 - S_1) \phi_{10}$ and $\phi_4 = v_2 (1 - S_2) \phi_{20}$. The corresponding fluid parameters for density, moduli, and viscosity of air, butane and water are calculated as 0.07g/cm³, 0.0037GPa, 0.009cP and 0.604g/cm³, 0.717GPa, 0.172cP and 1.033g/cm³, 2.45GPa, and 1.1cP.

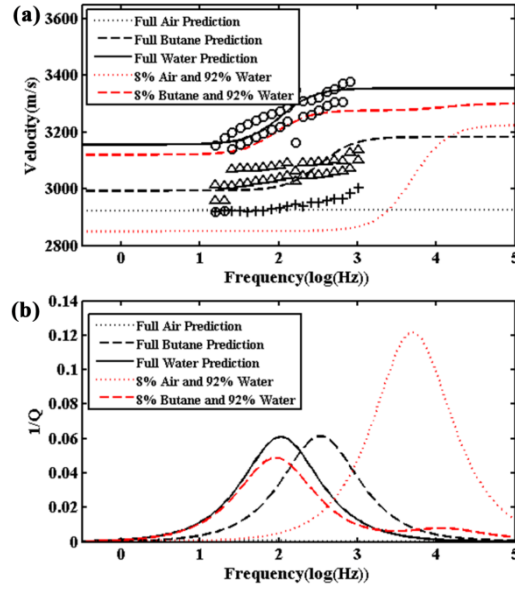


Figure 1: Theoretical prediction of fast compressional wave velocity (a) and attenuation (b) at different frequencies for the tight sandstone based on the DDP model. Low-frequency experimental data of compressional-wave velocity at full saturation are comparatively given in Figure 1a, where the open circles, the unfilled triangles and the crosses correspond to data at full-water, full-butane, and full-air saturation, respectively.

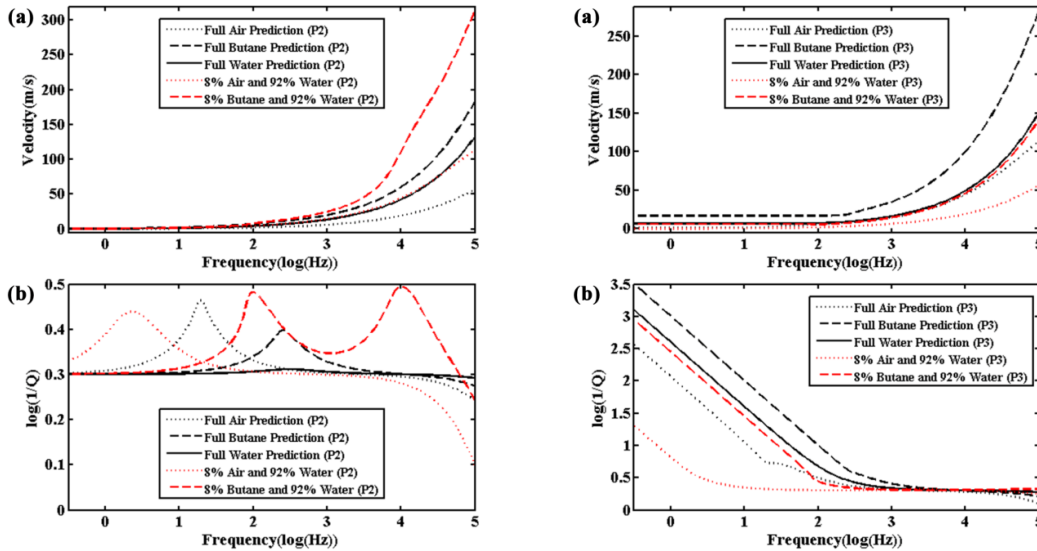


Figure 2: Theoretical prediction of the Biot slow P-wave (P2) velocity (a) and attenuation (b) at different frequencies for the fluid-saturated tight sandstone based on DDP model.

Figure 3: Theoretical prediction of the Biot slow P-wave (P3) velocity (a) and attenuation (b) at different frequencies for the fluid-saturated tight sandstone based on DDP model

Figure 1 shows the comparisons of compressional wave velocities between theoretical prediction and experimental data at different frequencies. As is shown in Figure 1, the experimental data of the low-frequency measurements at the three full saturation states all show very strong P-wave velocity dispersion and attenuation in the seismic band. And the theoretical prediction of DDP model exhibits an appropriate agreement with the experimental data, based on which the curves at partial saturation have also been predicted. The strong anelasticity in the seismic band should be a result of the mesoscopic heterogeneity. The peak values of the attenuation at full water saturation and full butane saturation are close, and the attenuation/dispersion at full water saturation happens at comparatively lower frequencies than that at full butane saturation. Regarding to the partial saturation curves, it can be observed that there are more than one attenuation peak and the characteristic frequency band of anelasticity caused by WILFF has been broadened. In the situation of air-water partial saturation, the peaks have merged due to coupling effect, and the patchy saturation in the inclusion skeleton dominates the anelasticity features, which strengthens the dissipation effect and causes the attenuation peak moving to the high frequencies compared with the full water saturation situation. While in the situation of butane-water partial saturation, the overlapping effect of fabric heterogeneity and patchy-saturation in the host skeleton causes the attenuation peak at $10^{1.9}$ Hz, and patchy-saturation in the inclusion skeleton leads to the attenuation peak at $10^{4.2}$ Hz.

The DDP model yields the four solutions of slow Biot compressional waves, and the wave velocity and attenuation curves of the two main compressional wave are showed in Figure 2 and Figure 3, respectively. P2 are caused by the friction effects between the host fluid in the host skeleton and solid and P3 are due to the effects between the host fluid in the inclusion skeleton and solid. Both Figure 2 and Figure 3 show that slow waves are highly diffusive.

CONCLUSIONS

A double double-porosity theoretical model has been presented to analyze the compressional wave dispersion and attenuation in the rocks where fabric heterogeneity and patchy-saturation coexist. This model can comprehensively describe the wave motion process of compressional waves in highly complex reservoir rocks. Comparisons between the theoretical prediction of fast compressional waves and the experimental data for a tight sandstone show good agreements, and correspondingly, the slow Biot waves are also predicted. The further applications of this model can help better revealing the quantitative relationships between wave anelasticity and lithologic properties in in-situ reservoir rocks.

ACKNOWLEDGMENTS

This work is sponsored by the Distinguished Professor Program of Jiangsu Province and the Fundamental Research Funds for the Central Universities, China.

REFERENCES

- Ba, J., J. M. Carcione, and J. Nie, 2011, Biot-Rayleigh theory of wave propagation in double-porosity media: *Journal of Geophysical Research: Solid Earth*, 116, B06202.
- Ba, J., L. Zhang, W. Sun, and H. Zhao, 2014, Velocity field of wave-induced local fluid flow in double-porosity media. *Science China-Physics: Mechanics & Astronomy*, 57, 1020-1030.
- Ba, J., Q. Du, J. M. Carcione, H. Zhang, and T. M. Müller, 2015, Seismic exploration of hydrocarbons in heterogeneous reservoirs: New theories, methods and applications, Elsevier Sci., Amsterdam.
- Ba, J., J. Zhao, J. M. Carcione, and X. Huang, 2016, Compressional wave dispersion due to rock matrix stiffening by clay squirt flow: *Geophysical Research Letters*, 43, 6186–6195.
- Batzle, M. L., D.-H. Han, and R. Hofmann, 2006, Fluid mobility and frequency-dependent seismic velocity—Direct measurements: *Geophysics*, 71, N1–N9.
- Dutta, N.C., and Hn. Odé, 1979, Attenuation and dispersion of compressional waves in fluid-filled porous rocks with partial gas saturation (White model), Part I-Biot theory: *Geophysics*, 44, 1777–1788.
- Mavko, G. M., and A. Nur, 1975, Melt squirt in the asthenosphere: *Journal Geophysical Research*, 80, 1444-1448.
- Pride, S. R., J. G. Berryman, and J. M. Harris, 2004, Seismic attenuation due to wave-induced flow: *Journal of Geophysical Research*, 109, B01201.
- Spencer, J. W., and J. Shine, 2016, Seismic wave attenuation and modulus dispersion in sandstones: *Geophysics*, 81, D211-D231.
- White, J. E., 1975, Computed seismic speeds and attenuation in rocks with partial gas saturation: *Geophysics*, 40, 224–232.